JOURNAL OF MAGNETIC RESONANCE **135,** 54–60 (1998)
ARTICLE NO. MN981530

A New Formalism for the Evaluation of Order-Fluctuation Modes in Liquid Crystals from Field-Cycling NMR-Relaxometry Data

F. Grinberg, R. Kimmich, R.-O. Seitter, and D. Pusiol*

*Sektion Kernresonanzspektroskopie, Universität Ulm, 89069 Ulm, Germany; and *Universidad Nacional de Córdoba, 5000 Córdoba, Argentina*

E-mail: farida.grinberg@physik.uni-ulm.de

Received August 12, 1997; revised March 24, 1998

A numerical procedure is presented which permits one to derive a formal distribution of collective fluctuation modes from experimental field-cycling NMR-relaxometry data of an ordered system. The purpose is to distinguish true order-fluctuation modes from local reorientation mechanisms. The evaluation scheme is demonstrated using simulated as well as experimental data. Applications serving the elucidation and characterization of modified or limited director fluctuation modes as they occur with liquid crystals in pores or with lyotropic systems are discussed. Test experiments have been carried out with a potassium laurate system. © 1998 Academic Press

Key Words: **spin–lattice relaxation; field-cycling relaxometry; liquid crystals; director fluctuations; mode relaxation rates.**

I. INTRODUCTION

Field-cycling NMR-relaxometry (*1–3*) has been used to probe collective molecular motions in liquid crystals. These motions represent a significant mechanism of spin–lattice relaxation in thermotropic liquid crystals at frequencies below 10^5–10^6 Hz. At higher frequencies, various types of non-collective motions due to translational diffusion and local molecular rotations typically dominate and tend to mask orientational director fluctuations (ODF) in the Megahertz regime. However, motional mechanisms (*4–13*) contributing to spin relaxation in lyotropic liquid crystals and biological membranes are less clear. In particular, slow non-collective motional dynamics competing with order fluctuations in the low frequency range might arise due to reorientations mediated by translational diffusion (*4, 6*) (RMTD) along the curved surface. These motions cannot be easily discriminated from ODF. A disputive point of discussion is also the appropriate modelling of collective fluctuations in bilayer membranes (*10–13*). Certain approaches (*10, 11*) are based on three-dimensional director fluctuations of the *nematic* type. In Ref. (*12*), however, two-dimensional layer undulations of (uncoupled) membranes were suggested as a fluctuation mechanism. Later the attention was drawn to the influence of layer coupling (*13*) in bilayer systems although it could not clearly be confirmed in experimental studies (*9*).

The discrimination of different NMR relaxation mechanisms is usually based on the identification of characteristic frequency dispersion laws of spin–lattice relaxation. Typical examples are the well known square-root and linear dispersion laws (*14–16*) reflecting director fluctuations of nematic and smectic crystals, respectively. However, such direct conclusions are only possible if the relaxation mechanism dominates in a wide frequency range so that the identification of a power law is unambiguous. Another approach employed for the interpretation of the experimental data is to fit model expressions for several superimposed relaxation mechanisms (*3, 6, 7, 17*). For example, frequency dependences of relaxation rates of thermotropic MBBA (*3*) (4-methoxybenzylidene-4′-n-butylaniline) and of lyotropic potassium-laurate water mixtures (*7*) in anisotropic phases were described in the range of $\approx 10^2$–10^8 Hz as a superposition of three processes due to (a) orientational director fluctuations, (b) local molecular rotation, and (c) molecular self-diffusion. The relaxation data of phospholipid membranes (*6*) in liquid crystalline phase were evaluated in terms of ODF, molecular rotation, "lateral" self-diffusion, and translationally induced rotations (RMTD). The problem of such procedures is that the choice of potential relaxation mechanisms tends to be ambiguous due to the big number of fitting parameters.

In this paper, we therefore suggest a different evaluation strategy. The idea is to translate the spin–lattice relaxation dispersion data into a formal distribution of director fluctuation modes irrespective of any additional motional components. Once having this formal distribution it would be much easier to distinguish true collective modes from contributions which in reality are due to local processes, and which are of minor interest in this context. After outlining the formal procedure, the evaluation will be demonstrated with simulated as well as experimental data.

II. EXPERIMENTAL

Spin–lattice relaxation times of protons in lyotropic mixture of potassium laurate/6.24% 1-decanol/68.6%D_2O were measured with a home-made field-cycling relaxometer. The detec-

1090-7807/98 $25.00
Copyright © 1998 by Academic Press
All rights of reproduction in any form reserved.

tion frequency for protons was about 60 MHz. The main contribution to spin–lattice relaxation arises from the protons of potassium laurate. The data refer to 318, 303, and 291 K. The phases occurring at these temperatures are classified (*18, 19*) as isotropic (ISO), nematic calamitic (N_c), and nematic discotic (N_d), respectively. The nematic phases are anisotropic in their diamagnetic susceptibilities, $\Delta\chi$, which is positive for N_c and negative for N_d. The nematic calamitic phase was shown (*19*) to contain elongated aggregates, whereas nematic discotic systems consist of oblate particles. The sizes of the aggregates and the system phase diagram are specified in Refs. (*18, 19*). It is worthwhile to note that the notation "isotropic phase" with respect to lyotropic liquid crystals refers to a totally disordered micellar packing, and must not to be confused with an isotropic molecular dispersion.

III. METHODICAL BACKGROUND

The Zeeman spin–lattice relaxation rate for a system of two dipolar-coupled spin $\frac{1}{2}$ nuclei separated by intermolecular distance r is given by

$$T_1^{-1} = \left(\frac{\mu_0}{4\pi}\right)^2 \frac{3}{20r^6}\gamma^4\hbar^2[\mathcal{J}(\omega_0) + 4\mathcal{J}(2\omega_0)], \qquad [1]$$

where μ_0 is the magnetic field constant, γ is the gyromagnetic ratio of protons, and $\hbar$ is Planck's constant divided by 2π. Motional spectral density $\mathcal{J}(\omega_0)$ at Larmor frequency ω_0 in Eq. [1] is

$$\mathcal{J}(\omega_0) = \int_{-\infty}^{\infty} G(t)e^{-i\omega_0 t}dt. \qquad [2]$$

The quantity $G(t)$ in Eq. [2] stands for the reduced dipolar auto-correlation function (see, for example, Ref. (*1*)) and reflects modulations of dipolar interactions by stochastic molecular motions. The relevant correlation function for relaxation by orientational director fluctuations is

$$G_{ODF}(t) = \langle \delta\boldsymbol{n}(\boldsymbol{r}, 0)\delta\boldsymbol{n}(\boldsymbol{r}, t)\rangle, \qquad [3]$$

where $\delta\boldsymbol{n}(\boldsymbol{r}, t)$ denotes the fluctuation of the instantaneous director $\boldsymbol{n}(\boldsymbol{r}, t)$ at each moment of time t apart from the equilibrium value $\langle\boldsymbol{n}\rangle$

$$\delta\boldsymbol{n}(\boldsymbol{r}, t) = \boldsymbol{n}(\boldsymbol{r}, t) - \langle\boldsymbol{n}\rangle. \qquad [4]$$

(Numerical coefficients connecting correlation functions $G(t)$ and $G_{ODF}(t)$ can be found for instance in Ref. (*20*).) The contribution of ODF to the intensity function is then given by the term (*16, 21*)

$$\mathcal{J}(\omega_0) = S^2\Re e \int_{-\infty}^{\infty} \langle \delta\boldsymbol{n}(\boldsymbol{r}, 0)\delta\boldsymbol{n}(\boldsymbol{r}, t)\rangle e^{-i\omega_0 t}dt, \qquad [5]$$

where S is the nematic order parameter (*22*), the equilibrium director is supposed to be oriented along the external magnetic field parallel to the z-axis of the Cartesian coordinate system, and the internuclear vector parallel to the long molecular axes.

Director fluctuations are usually expressed in terms of their Fourier components in the reciprocal space

$$\delta\boldsymbol{n}(\boldsymbol{r}, t) = \frac{1}{V}\sum_{\boldsymbol{q}} \delta\boldsymbol{n}(\boldsymbol{q}, t)e^{-i\boldsymbol{q}\boldsymbol{r}}, \qquad [6]$$

where V is the sample volume and $\boldsymbol{q}$ is the wave vector.

Fluctuation modes $\delta\boldsymbol{n}(\boldsymbol{q}, t)$ relax with exponential damping (*22*) with rates $\tau^{-1}(\boldsymbol{q})$

$$\delta\boldsymbol{n}(\boldsymbol{q}, t) = \delta\boldsymbol{n}(\boldsymbol{q}, 0)e^{-(|t|/\tau(\vec{q}))}. \qquad [7]$$

The correlation function $G_{ODF}(t)$ thus represents a superposition of overdamped relaxation processes with a broad distribution of mode relaxation rates

$$G(t) = \int_0^{\infty} P(\tau^{-1})e^{-(|t|/\tau)}\, d\tau^{-1}, \qquad [8]$$

where $P(\tau^{-1})$ is the weight function of fluctuation relaxation rates.

Using Eq. [8] and carrying out the time integration the intensity function, Eq. [2], reduces to

$$\mathcal{J}(\omega_0) = \int_{-\infty}^{\infty} P(\tau^{-1})\frac{2\tau^{-1}}{\omega_0^2 + \tau^{-2}}\, d\tau^{-1}. \qquad [9]$$

Our approach is now based on the reconstruction of the distribution function $P(\tau^{-1})$ using the numerical fit of Eqs. [9], [1] to experimental data $T^{-1}(\omega_0)$. The NNLS (nonnegatively constrained least-squares) fitting procedure (*23*) has been used (see also Ref. (*24*)). The integration in Eq. [9] is replaced by the summation over the limited range from a certain minimal (τ_{min}^{-1}) up to a certain maximal (τ_{max}^{-1}) value of the relaxation rate

$$\mathcal{J}(\omega_0) \approx \sum_{\tau_{min}^{-1}}^{\tau_{max}^{-1}} P_i(\tau_i^{-1})\frac{2\tau_i^{-1}}{\omega_0^2 + \tau_i^{-2}}\,\Delta\tau_i^{-1}. \qquad [10]$$

The reliability of the fitting procedure was at first proved for the simple case of a distribution $P(\tau^{-1})$ consisting of only one

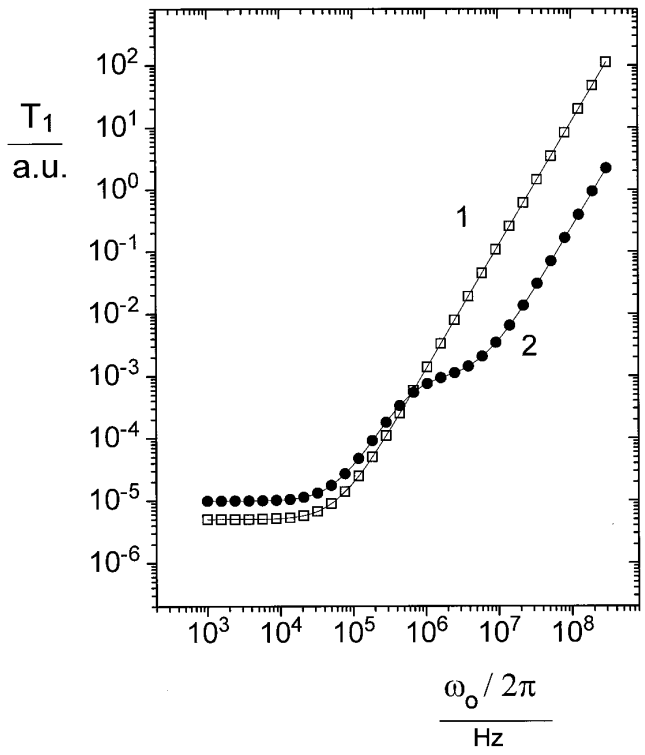

FIG. 1. Frequency dependences of the spin–lattice relaxation time simulated according to Eqs. [1], [10]. Curve 1 corresponds to Eq. [10] for a single sum term with $\tau^{-1} = 2\pi 10^5\ s^{-1}$. Curve 2 corresponds to two equally weighted sum terms in Eq. [10] with $\tau_1^{-1} = 2\pi 10^5\ s^{-1}$ and $\tau_2^{-1} = 2\pi 10^7\ s^{-1}$. The solid lines represent fits of Eqs. [1], [9].

or two discrete terms. The dispersion curves simulated using Eqs. [1] and [10] are shown in Fig. 1. Curve 1 corresponds to a single sum term, Eq. [10], with $\tau^{-1} = 2\pi 10^5\ s^{-1}$. Curve 2 was calculated from two equally weighted terms with $\tau_1^{-1} = 2\pi 10^5\ s^{-1}$ and $\tau_2^{-1} = 2\pi 10^7\ s^{-1}$. Corresponding values obtained in the fitting procedure differed from those used in the simulations by not more than 1–2%.

IV. SIMULATED T_1-DISPERSION CURVES FOR ODF

In the frame of classical continuum theory of liquid crystals (*22*) and using Eqs. [6], [7] the intensity function, Eq. [5], reduces to (*16, 21*)

$$\mathcal{J}(\omega_0) = \frac{1}{V^2} S^2 \sum_{\boldsymbol{q}} \sum_{\alpha=1}^{2} \langle |\delta n_\alpha(\boldsymbol{q}, 0)|^2 \rangle \frac{2\tau_\alpha^{-1}(\boldsymbol{q})}{\omega_0^2 + \tau_\alpha^{-2}(\boldsymbol{q})}. \quad [11]$$

The $\delta n_\alpha(\boldsymbol{q}, t)$ are two uncoupled components (*22*) of normal mode $\delta \boldsymbol{n}_\alpha(\boldsymbol{q}, t)$ in two perpendicular directions within the (x, y) plane. These modes are indicative for proper diagonalization of free energy expressions. The mean square amplitudes of the transverse modes and their relaxation rates are (*22*)

$$\langle |n_\alpha(\boldsymbol{q}, 0)|^2 \rangle = \frac{k_B T V}{K_\alpha(\boldsymbol{q})} \quad [12]$$

$$\tau_\alpha^{-1}(\boldsymbol{q}) = \frac{K_\alpha(\boldsymbol{q})}{\eta_\alpha(\boldsymbol{q})}, \quad [13]$$

where

$$K_\alpha(\boldsymbol{q}) = K_{\alpha\alpha}(q_x^2 + q_y^2) + K_{33} q_z^2 + \Delta\chi B^2 \quad [14]$$

and $\eta_\alpha(\boldsymbol{q})$ are the effective viscosities, T is the temperature, and k_B is Boltzman's constant. Quantities K_{11}, K_{22}, and K_{33} in Eq. [14] are three basic elastic constants associated with splay, twist and bend, respectively, and B is the magnetic-flux density. In the following the magnetic-field term and the wave vector dependence of the viscosities will be ignored for simplicity. Replacing a sum over q-values in Eq. [11] by an integration and using Eqs. [12], [13] gives

$$\mathcal{J}(\omega_0) = \frac{S^2 k_B T}{(2\pi)^3} \sum_{\alpha=1}^{2} \int_{-(2\pi/\lambda_c)}^{2\pi/\lambda_c} \int_{-(2\pi/\lambda_c)}^{2\pi/\lambda_c} \int_{-(2\pi/\lambda_c)}^{2\pi/\lambda_c} \times \frac{1}{\eta_\alpha \tau_\alpha^{-1}(\boldsymbol{q})} \frac{2\tau_\alpha^{-1}(\boldsymbol{q})}{\omega_o^2 + \tau_\alpha^{-2}(\boldsymbol{q})} dq_x dq_y dq_z, \quad [15]$$

where the integration limits are determined by the high-frequency cutoff of the continuum theory (λ_c is the characteristic wave length large compared to the molecular size). Clearly, according to Eqs. [15], [13], and [14] the contribution of director fluctuation modes to the spin–lattice relaxation rate depends on anisotropic properties (*20, 21, 25*) of the elasticity tensor. In the case of nematics the anisotropy of the elastic constants is usually ignored (isotropic three-dimensional director fluctuations) and a one-constant approximation is considered to be adequate ($K_{33} = K_{11} = K_{22}$). In essentially two-dimensional systems (bilayer membranes, smectics in absence of the coupling between layers) anisotropic properties become most important since allowed deformations lie within the transverse plane (undulation modes). In the case of completely uncoupled layers K_{33} can be set to zero.

In the following we consider the case $K_{33} \leq K_{11}, K_{22}$. The problem is now to rewrite Eq. [15] in a form suitable for an evaluation of the distribution function $P(\tau^{-1})$ as defined by Eq. [9]. This can be done by introducing new variables $\tilde{q}_{x\alpha} = \sqrt{(K_{\alpha\alpha}/\eta_\alpha)}\, q_x$, $\tilde{q}_{y\alpha} = \sqrt{(K_{\alpha\alpha}/\eta_\alpha)}\, q_y$, $\tilde{q}_{z\alpha} = \sqrt{(K_{33}/\eta_\alpha)}\, q_z$ and carrying out the integration in polar coordinates over the volume of a rotational ellipsoid (*25*) (with the axis in the z-direction equal to $2(2\pi/\lambda_c)\sqrt{(K_{33}/\eta_\alpha)}$ and two axes in the perpendicular plane equal to $2(2\pi/\lambda_c)\sqrt{(K_{\alpha\alpha}/\eta_\alpha)}$). The result is

$$\mathcal{I}(\omega_0) = \frac{S^2 k_B T}{(2\pi)^2}\left\{\sum_{\alpha=1}^{2}\frac{\sqrt{\eta_\alpha}}{K_{\alpha\alpha}\sqrt{K_{33}}}\left[\int_0^{(2\pi/\lambda_c)^2 K_{33}/\eta_\alpha} \times \frac{1}{\sqrt{\tau_\alpha^{-1}(\boldsymbol{q})}}\frac{2\tau_\alpha^{-1}(\boldsymbol{q})}{\omega_0^2+\tau_\alpha^{-2}(\boldsymbol{q})}\,d\tau_\alpha^{-1}(\boldsymbol{q}) + \int_{(2\pi/\lambda_c)^2 K_{33}/\eta_\alpha}^{(2\pi/\lambda_c)^2 K_{\alpha\alpha}/\eta_\alpha} \frac{1}{\sqrt{\tau_\alpha^{-1}(\boldsymbol{q})}} \times \sqrt{\frac{1/\tau_\alpha^{-1}(\boldsymbol{q}) - 1/(2\pi/\lambda_c)^2\,(K_{\alpha\alpha}/\eta_\alpha)}{1/(2\pi/\lambda_c)^2\,(K_{33}/\eta_\alpha) - 1/(2\pi/\lambda_c)^2\,(K_{\alpha\alpha}/\eta_\alpha)}} \times \frac{2\tau_\alpha^{-1}(\boldsymbol{q})}{\omega_0^2+\tau_\alpha^{-2}(\boldsymbol{q})}\,d\tau_\alpha^{-1}(\boldsymbol{q})\right]\right\}$$

$$= \frac{S^2 k_B T}{(2\pi)^2}\sum_{\alpha=1}^{2}\frac{\sqrt{\eta_\alpha}}{K_{\alpha\alpha}\sqrt{K_{33}}}\int_0^{(2\pi/\lambda_c)^2 K_{\alpha\alpha}/\eta_\alpha} \times P_\alpha(\tau_\alpha^{-1}(\boldsymbol{q}))\frac{2\tau_\alpha^{-1}(\boldsymbol{q})}{\omega_0^2+\tau_\alpha^{-2}(\boldsymbol{q})}\,d\tau_\alpha^{-1}(\boldsymbol{q}), \qquad [16]$$

where

$$P_\alpha(\tau_\alpha^{-1}(\boldsymbol{q})) = \begin{cases} \dfrac{1}{\sqrt{\tau_\alpha^{-1}(\boldsymbol{q})}}, & 0 \le \tau_\alpha^{-1}(\boldsymbol{q}) < \left(\dfrac{2\pi}{\lambda_c}\right)^2\dfrac{K_{33}}{\eta_\alpha} \\ \dfrac{1}{\sqrt{\tau_\alpha^{-1}(\boldsymbol{q})}}\sqrt{\dfrac{1/\tau_\alpha^{-1}(\boldsymbol{q}) - 1/(2\pi/\lambda_c)^2\,K_{\alpha\alpha}/\eta_\alpha}{1/(2\pi/\lambda_c)^2\,K_{33}/\eta_\alpha - 1/(2\pi/\lambda_c)^2\,K_{\alpha\alpha}/\eta_\alpha}}, & \left(\dfrac{2\pi}{\lambda_c}\right)^2\dfrac{K_{33}}{\eta_\alpha} \le \tau_\alpha^{-1}(\boldsymbol{q}) < \left(\dfrac{2\pi}{\lambda_c}\right)^2\dfrac{K_{\alpha\alpha}}{\eta_\alpha} \end{cases}. \qquad [17]$$

A graphical representation of Eq. [17] is given in Fig. 2. Limits of Eq. [17] are:

Case 1. $K_{33} = K_{\alpha\alpha} = K$; $\eta_1 = \eta_2 = \eta$.

$$P_\alpha(\tau_\alpha^{-1}(\boldsymbol{q})) = (\tau^{-1}(\boldsymbol{q}))^{-0.5}. \qquad [18]$$

Case 2. $K_{33} = 0$.

$$P_\alpha(\tau_\alpha^{-1}(\boldsymbol{q})) = (\tau_\alpha^{-1}(\boldsymbol{q}))^{-1}, \quad \tau_\alpha^{-1}(\boldsymbol{q}) \ll \left(\frac{2\pi}{\lambda_c}\right)^2\frac{K_{\alpha\alpha}}{\eta_\alpha}. \qquad [19]$$

The integration of Eq. [16] in Cases 1 and 2 is straightforward and leads in the low-frequency limit to well-known dispersion laws (*14–16*) $T_1 \propto \omega_o^\beta$ with $\beta = 0.5$ in Case 1 and $\beta = 1$ in Case 2.

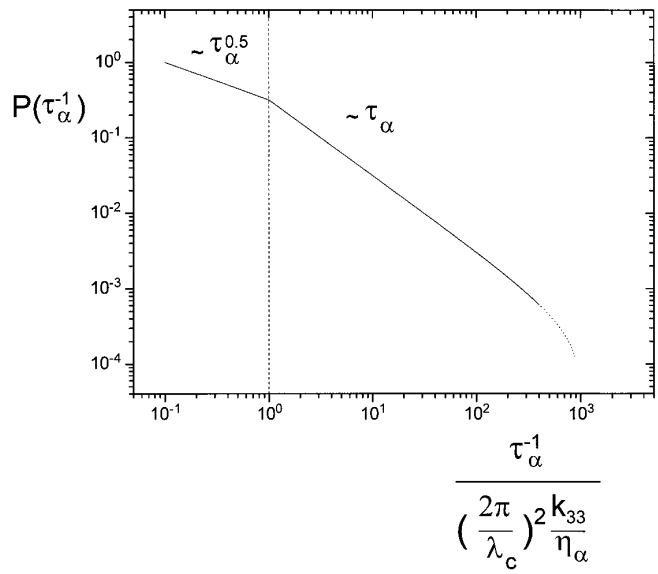

FIG. 2. Graphical representation of Eq. [17] for $K_{\alpha\alpha}/K_{33} = 1000$.

Figure 3a shows $P(\tau^{-1})$ as reconstructed by fitting Eqs. [9], [1] to simulated dispersion curves in both limiting cases. (The differences expressed by index α have been ignored. This corresponds to the case of either equal constants K_{11} and K_{22} or one of them being equal to zero.) The simulated dispersion curves are shown in Fig. 3b together with their fits (solid lines). Reconstructed functions $P(\tau^{-1})$ in Fig. 3a are in a good agreement with the model predictions, Eqs. [18] and [19], represented graphically by solid lines.

Another example demonstrates the reconstruction of the function $P(\tau^{-1})$ for the case that the intensity function $\mathcal{I}(\omega_0)$ represents a sum of two discrete and one "continuous" ($\propto 1/\omega_0$) contributions, that is,

$$\mathcal{I}(\omega_0) = C_1\frac{2\tau_1^{-1}}{\omega_0^2+\tau_1^{-2}} + C_2\frac{2\tau_2^{-1}}{\omega_0^2+\tau_2^{-2}} + C_3\frac{1}{\omega_0}. \qquad [20]$$

Figure 4a shows the dispersion curve simulated using Eqs. [1], [20] with $\tau_1^{-1} = 2\pi 10^6\ s^{-1}$, $\tau_2^{-1} = 2\pi 10^8\ s^{-1}$, and C_1

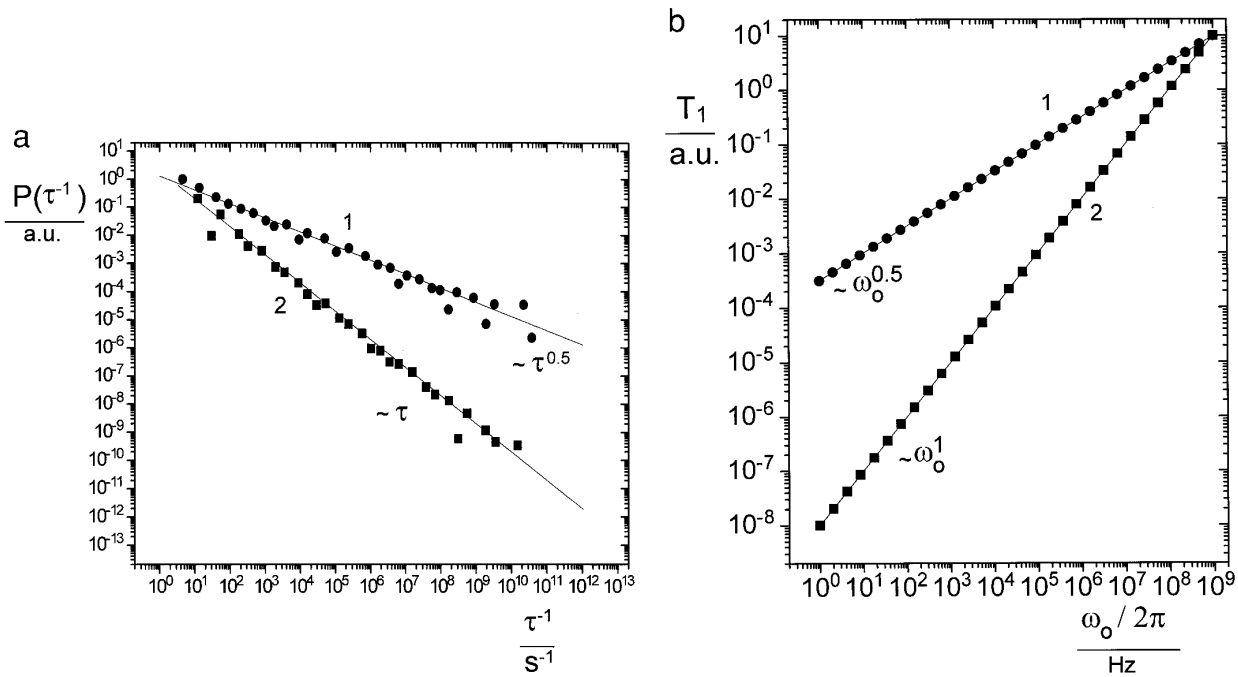

FIG. 3. (a) $P(\tau^{-1}(\boldsymbol{q}))$ obtained by fitting Eqs. [1], [9] to the T_1-dispersion curves shown in Fig. 3b. The numbers indicate the correspondence of the curves in Figs. 3a and 3b. The solid lines represent Eqs. [18] (curve 1) and [19] (curve 2). (b) Frequency dependences of the spin–lattice relaxation time simulated according to $T_1 \propto \omega_o^{\beta}$ with $\beta = 0.5$ (curve 1) and $\beta = 1$ (curve 2). The solid lines represent fits of Eqs. [1], [9] to the data points. The fitted distributions $P(\tau^{-1}(\boldsymbol{q}))$ are shown in Fig. 3a.

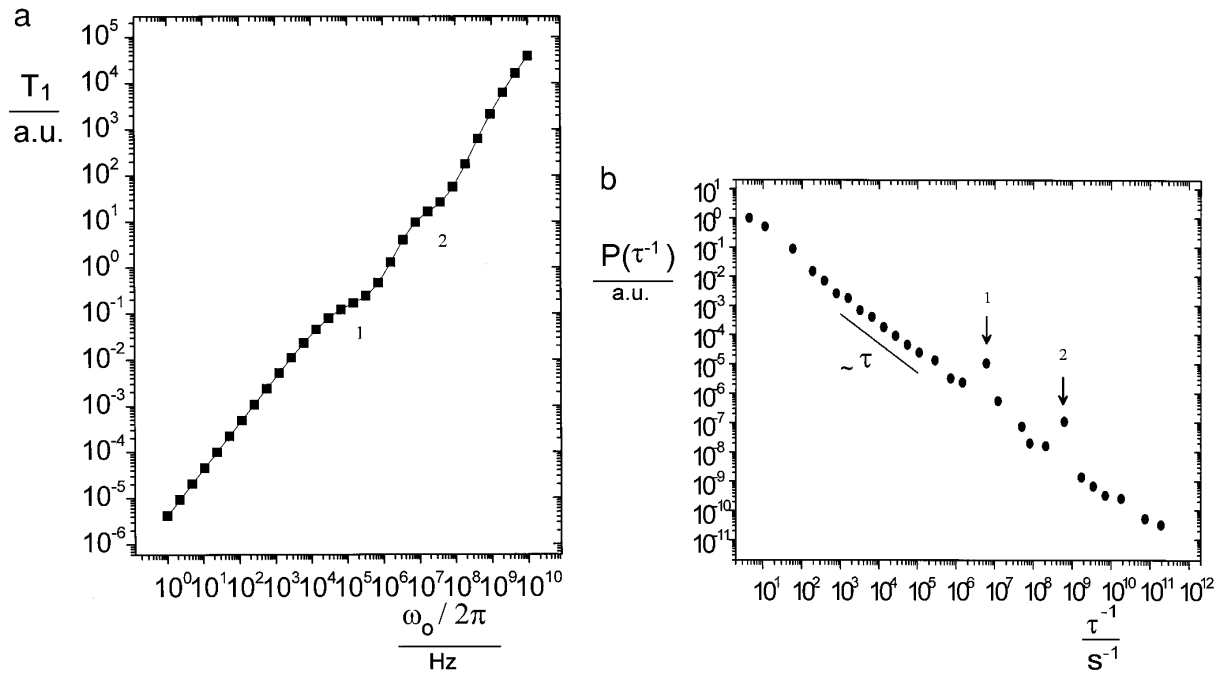

FIG. 4. (a) Frequency dependence of the spin–lattice relaxation time simulated using Eqs. [1], [20] with $\tau_1^{-1} = 2\pi 10^6\ s^{-1}$, $\tau_2^{-1} = 2\pi 10^8\ s^{-1}$ and $C_1 = C_2 = 0.46$, $C_3 = 0.08$. The solid line was calculated based on the fit of Eqs. [1], [9] to the data points. The fitted function $P(\tau^{-1}(\boldsymbol{q}))$ is shown in Fig. 4b. (b) $P(\tau^{-1})$ obtained by fitting Eqs. [1], [9] to the T_1-dispersion curve shown in Fig. 4a. (The function $P(\tau^{-1})$ in this case is not the true probability function, since we have omitted the proportionality coefficient in $\mathcal{J}(\omega_0) \propto 1/\omega_0$ for simplicity when simulating the dispersion curve.)

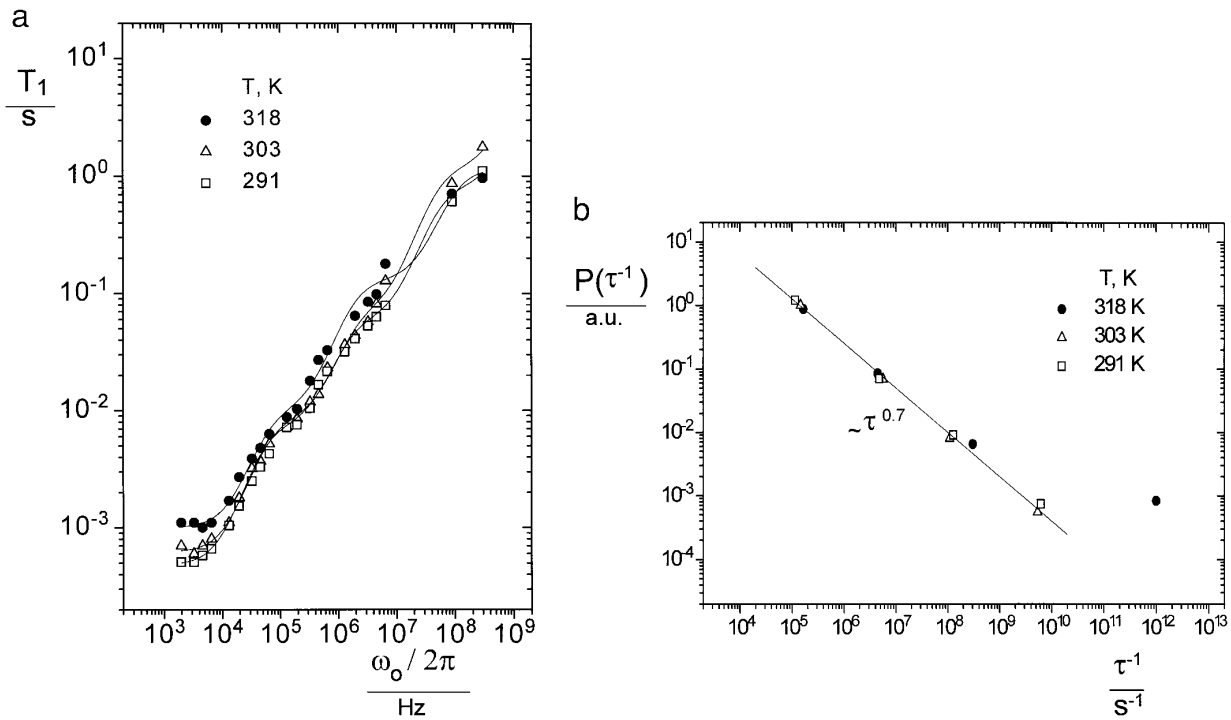

FIG. 5. (a) Frequency dependences of the proton spin–lattice relaxation time in the system potassium laurate/6.24% 1-decanol/68.6%D_2O. The solid lines represent fits of Eqs. [1], [9] to the data points. The fitted distributions $P(\tau^{-1}(\boldsymbol{q}))$ are shown in Fig. 5b. (b) Fitted distributions $P(\tau^{-1}(\boldsymbol{q}))$ derived from the T_1-dispersion curves of potassium laurate/6.24% 1-decanol/68.6%D_2O shown in Fig. 5a. The solid line represents a power-law function $P(\tau^{-1}) \propto (\tau)^{\kappa}$ with $\kappa = 0.7$.

$= C_2 = 0.46$, $C_3 = 0.08$. The discrete contributions produce the distorted regions 1 and 2 in the dispersion curve. The weighting constants, C_1, C_2, C_3, were used in order to obtain a reasonable shape of the simulated dispersion curve. The fitted function $P(\tau^{-1})$ is shown in Fig. 4b. It reproduces the expected slope given by Eq. [19] and contains two peaks at $\tau^{-1} = 6.05 \times 10^6\ s^{-1}$ and $6.24 \times 10^8\ s^{-1}$ that are in a good agreement with the values τ_1^{-1} and τ_2^{-1} assumed for the simulation. The solid line in Fig. 4a was recalculated based on the evaluated distribution function $P(\tau^{-1})$ and gives a good representation of the original data points.

V. EXPERIMENTAL T_1-DISPERSION DATA OF LYOTROPIC LIQUID CRYSTALS

Spin–lattice relaxation of a lyotropic mixture of potassium laurate/6.24% 1-decanol/68.6%D_2O was studied in three different phase states: ISO, N_c, and N_d. Dispersion curves measured, respectively, at 318, 303, and 291 K are shown in Fig. 5a. The fits of Eqs. [9], [1] to experimental dependences $T_1(\omega_0)$ are represented by solid lines. The fitted distribution functions $P(\omega^{-1})$ are shown in Fig. 5b. They can be empirically described by a power-law function $P(\tau^{-1}) \propto (\tau^{-1})^{\kappa}$ with $\kappa = -0.7$. The obtained value of κ does not coincide with any of the values corresponding to the limiting three-dimensional ($\kappa = -0.5$) and two-dimensional ($\kappa = -1$) cases, see Eqs. [18], [19]. The same value of κ was observed in isotropic and both nematic phases which differentiate by the type of ordering of individual aggregates. Any coupling between aggregates thus must be negligible.

VI. DISCUSSION AND CONCLUSIONS

Field-cycling relaxometry data permits one to reconstruct the distribution function of mode relaxation rates in liquid crystals, $P(\tau^{-1})$, using the numerical fit of Eqs. [9], [1] to the experimental dependences $T^{-1}(\omega_0)$. This function is of basic importance for the understanding of the dynamical properties of the system, and can be compared, where available, to analytical results. A good agreement of reconstructed functions $P(\tau^{-1})$ with predictions of classical theories was demonstrated, Fig. 3a, using simulated dispersion curves in two limiting cases: isotropic three-dimensional and essentially two-dimensional order fluctuations. With respect to real objects the method is expected to visualize frequency ranges of validity of theory predictions and that of any deviations. This is expected to be important for the investigation of microconfined nematic crystals and for handling the problems of low frequency cutoffs imposed on ODF by finite pore sizes, for instance.

The two-dimensional case resulting in the linear dependence of the distribution function $P(\tau^{-1})$ on $1/\tau^{-1}(\boldsymbol{q})$, Eq. [19], is assumed (*12*) to reflect surface undulations of biological mem-

branes and thus must be relevant for a big but unsufficiently explored field of investigations. Our first study of lyotropic mixtures of potassium laurate/6.24% 1-decanol/68.6%D_2O, however, did not give the evidence for any non-negligible contribution of director fluctuation modes within the investigated frequency range. This conclusion is based on the observation of similar behaviour of experimental dependences $T_1(\omega_0)$, Fig. 5a, as well as of evaluated functions $P(\tau^{-1})$, Fig. 5b, both in isotropic and anisotropic phases. Besides, the fitted value $\kappa = -0.7$ of function $P(\tau^{-1}) \propto (\tau^{-1})^{\kappa}$ does not concide with the predicted value $\kappa = -1$, Eq. [19].

The absence of essential differences in isotropic and nematic phases suggests that strong T_1-dispersions observed in the whole frequency range down to a few KHz must reflect rather slow internal motional processes associated with individual molecular aggregates. These motions may be of a rather complicated nature. A suitable basis for discussion might be, for example, the RMTD (*4*) which in principle could also be analysed in terms of Eq. [9]. This is to be considered in future discussions along with systematic experimental studies of systems at various concentrations of amphiphilic molecules.

The reconstruction of $P(\tau^{-1})$ directly from field-cycling relaxometry data promises to be particularly useful in cases when director fluctuations are to be distinguished from non-collective relaxation mechanisms. Note that if several mechanisms each dominating in a certain frequency range are superimposed, their contributions to $P(\tau^{-1})$ appear separately whereas they reveal themselves in the relaxation dispersion curves in a much less distinct manner. That is, the concrete knowledge and parameter fits of all contributing mechanisms are not required. A certain analogy can be seen here with the analysis of FIDs in terms of Fourier transformed spectra. The FIDs contain the same information as the spectra, of course, but cannot directly be "read."

Although field-cycling relaxometry has proved to be an efficient tool for the elucidation of ODF in liquid crystals, an unambiguous discrimination of collective and non-collective molecular motions on the basis of field-cycling relaxometry exclusively was not always possible. New perspectives were recently recognized in a favourable combination of field-cycling relaxometry and a new experiment based on the dipolar-correlation effect (*26–29*) (DCE) which is extremely sensitive to the order and ODF. The DCE permits one to monitor dipolar correlations in the time scale from $\approx 10^{-4}$ s up to the order of spin–lattice relaxation times. This extends the low frequency range of the field-cycling relaxometry by an additional 3 orders. The evaluation of T_1-dispersion data in terms of $P(\tau^{-1})$ can thus be compared with the distribution derived from DCE data.

ACKNOWLEDGMENTS

We thank Dr. S. Stapf for providing computer programms, Dr. R. Rodriguez for preparing samples, the DAAD (Germany), and the Fundación Antorchas (Argentina) for financial support.

REFERENCES

1. R. Kimmich, "NMR: Tomography, Diffusometry, Relaxometry," Springer-Verlag, Heidelberg (1997).
2. F. Noack, *Progr. NMR Spectrosc.* **18,** 171 (1986).
3. F. Noack, M. Notter, and W. Weiss, *Liquid Crystals* **3,** 907 (1988).
4. R. Kimmich and H. W. Weber, *Phys. Rev. B* **47,** 11,788 (1993).
5. R. Kimmich, G. Schnur, and A. Scheuermann, *Chem. Phys. Lipids* **32,** 271 (1983).
6. E. Rommel, F. Noack, P. Meier, and G. Kothe, *J. Phys. Chem.* **92,** 2981 (1988).
7. W. Kühner, E. Rommel, F. Noack, and P. Meier, *Z. Naturforsch. A* **42,** 127 (1987).
8. J. Stohrer, G. Gröbner, D. Reimer, K. Weisz, C. Mayer, and G. Kothe, *J. Chem. Phys.* **95,** 672 (1991).
9. J. Struppe, F. Noack, and G. Klose, *Z. Naturforsch. A* **52,** 681 (1997).
10. M. F. Brown, *J. Chem. Phys.* **80,** 2808 (1984).
11. M. F. Brown, J. F. Ellena, C. Trindle, and G. D. Williams, *J. Chem. Phys.* **84,** 465 (1986).
12. J. A. Marqusee, M. Warner, and K. Dill, *J. Chem. Phys.* **81,** 6404 (1984).
13. B. Halle, *Phys. Rev. E* **50,** R2415 (1994).
14. P. Pincus, *Solid State Commun.* **7,** 415 (1969).
15. R. Blinc, D. L. Hogenboom, D. E. O'Reilly, and E. M. Peterson, *Phys. Rev. Lett.* **23,** 969 (1969).
16. R. Blinc, M. Luzar, M. Vilfan, and M. Burgar, *J. Chem. Phys.* **63,** 3445 (1975).
17. D. Pusiol and F. Noack, *Liquid Crystals* **5,** 377 (1989).
18. A. M. Figueiredo Neto, L. Liébert, and Y. Galerne, *J. Phys. Chem.* **89,** 3737 (1985).
19. Y. Hendrikx, J. Charvolin, M. Rawiso, L. Liébert, and M. C. Holmes, *J. Phys. Chem.* **87,** 3991 (1983).
20. R. Blinc, *NMR Basic Princ. Prog.* **13,** 97 (1976).
21. M. Vilfan, M. Kogoj, and R. Blinc, *J. Chem. Phys.* **86,** 1055 (1987).
22. P. G. de Gennes, "The Physics of Liquid Crystals," Clarendon, Oxford (1974).
23. R. S. Sacher and I. D. Morrison, *J. Colloid Interface Sci.* **70,** 153 (1979).
24. S. Stapf, R. Kimmich, and R.-O. Seitter, *Phys. Rev. Lett.* **75,** 2885 (1995).
25. R. R. Vold and R. L. Vold, *J. Chem. Phys.* **88,** 4655 (1988).
26. R. Kimmich, E. Fischer, P. Callaghan, and N. Fatkullin, *J. Magn. Reson. A* **117,** 53 (1995).
27. F. Grinberg and R. Kimmich, *J. Chem. Phys.* **103,** 365 (1995).
28. F. Grinberg and R. Kimmich, *J. Chem. Phys.* **105,** 3301 (1996).
29. F. Grinberg, R. Kimmich, M. Möller, and A. Molenberg, *J. Chem. Phys.* **105,** 9657 (1996).